An Experimental Study on the Dynamics of Binder Drops Impacting on a Powder Surface in Binder Jetting Additive Manufacturing

Zachary Pakulniewicz ¹ and Yang Liu² (\boxtimes)

Department of Mechanical Engineering, City College of New York, New York, NY, 10031, USA

Binder jetting additive manufacturing (AM) is an innovative form of 3D printing that generates complex and advanced structures of various materials by jetting binder drops onto a powder bed. The drops on the bed cure the powder to form structures in a quick and efficient manner. However, the method suffers several flaws including manufacturing inconsistencies and coarse resolution of structures. These flaws may be explained by complex interactions between the binder drop and the powder during the printing process. Therefore, a better understanding of these interactions will be instrumental in the development of binder jetting for fabricating multipurpose, higher quality functional structures. In this study, these complex interactions are analyzed during the impact and subsequent processes. The impact dynamics of binder drops on a powder surface were examined by using a custom impingement rig under various test conditions (i.e., different impact velocities and binder viscosities). A high-speed imaging system was used to capture the transient details of the drop-powder interactions. This study concludes that an increase in drop impact velocity results in a greater range of particle ejection. A lower drop viscosity results in a higher dry spread of particles while a higher drop viscosity results in a greater number of binder-encapsulated particles. Across all cases, binder drops absorb particle granules at a rate inverse to their viscosity.

I. Introduction

Additive manufacturing (AM) has quickly become one of the most lucrative industrial markets of the modern era. This process is commonly referred to as "3D printing" and generally involves the jetting of a material in three axes to create a physical structure [1]. The AM printer is instructed by a reference CAD file on the selective jetting process to fabricate the structure. There are many methods of AM that have established prominence over the last few years, including stereolithography (SLA), selective laser sintering (SLS), and fused deposition modeling (FDM). However, many of these technologies suffer from a lack of versatility [2]. The most common AM techniques are limited by a lack of variety in printing material and the inability to print at room-temperature and standard atmospheric pressure [3]. Thus, a new technology is desired which can operate under such conditions; binder jetting AM is one such solution to the conditional limitations.

Binder jetting AM operates as all other AM technologies do in that it involves selective jetting over a surface to create a structure. Conversely to the other methods, binder jetting jets a liquid onto a powder of the material that is desired to be printed from [4]. The liquid used by the printer is called a *binder drop*, a drop of DI-water which contains a binding agent to increase its viscosity. The selective jetting of binder drops allows for the adhesion of the material powder in the printing bed to take the form as the desired shape [4]. A piston rolls a fresh layer of powder over the bed as the process is repeated. Upon the evaporation of the binder drop, the manufacturer is left with a product of their desired material gelled together.

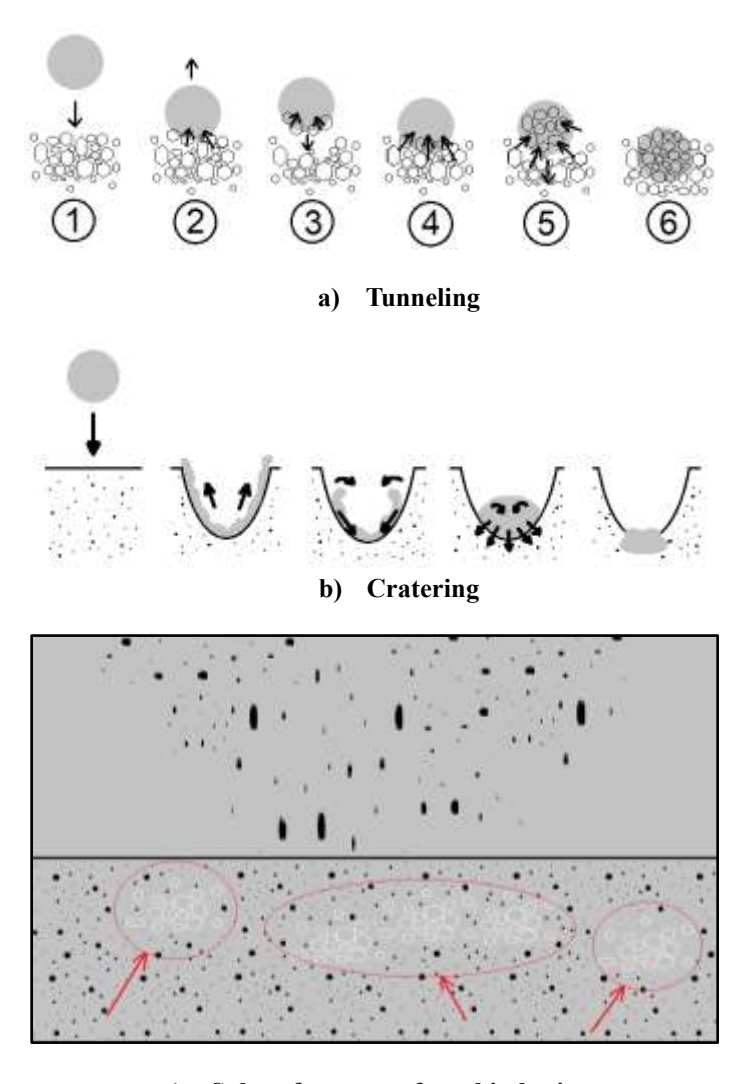
Unfortunately, limited research of binder jetting has left the technology with some unresolved flaws in manufacturing. Binder jetted structures often suffer from a lower relative density and higher surface porosity from the powdered material it is constructed of [4]. Consequently, post-processing steps such as densification or curing are applied to the structure [5]. These post-processing steps may result in a significant distortion of the structure geometry and experience lower mechanical properties than that of structures manufactured using the SLS technique.

These limitations are caused by multiple factors. One such theory is that extrinsic properties of the power (such as porosity) result in the nonuniform and variable impact of binder drop [4]. These interactions can include tunneling and cratering of the binder drop into the powder as shown in Fig. 1(a) and (b), each causing variation in geometry. It

¹Undergraduate Research Assistant at the Department of Engineering of ECU

²Assistant Professor at the Department of Mechanical Engineering of CCNY, Email: yliu7@ccny.cuny.edu

is also observed that the impact of a binder drop onto a powder bed creates an ejection of powder particles, forming pores beneath the surface of the powder [6,7] as illustrated in Fig. 1(c).



c) Subsurface pores from binder impact

Figure 1: Different effects of binder drop impact on powder surfaces. A) Tunneling phenomenon of binder drop, characterized by absorption of powder, B) Cratering phenomenon, characterized by the indention of the binder drop, and C) Pores formed under the surface after binder impact.

A better understanding of the micro-physical details during the impact of the binder drops and the interactions between the binder drop and powder is strongly desired to help minimize these flaws during the printing process. This study will specifically focus on the effects of binder viscosity and impact velocity on the impacting dynamics of the binder drop on a powder surface.

In the present study, a comprehensive experimental study was carried out to evaluate the effects of the binder liquid viscosity and droplet impact velocity on the impacting dynamics (i.e., spreading, receding, and rebounding) and the consequent drop-powder interactions (i.e., ejection and encapsulation) during the binder jetting printing process. The test materials and the experimental setup are illustrated first. Then, the experimental results of high-speed imaging of binder drop impacting on the powder surface under various impact velocities and binder viscosities are compared in detail. An image-processing technique is also introduced to extract the important parameters of drop-powder interactions during the impacting processes. Finally, the effects of drop impact velocity and the binder viscosity on the powder particle ejection dynamics are discussed.

II. Materials and Methods

Although binder research is a novelty topic, there have been numerous studies that have prompted the discussion on binder-powder interactions. The following materials were inspired by the work of Rajniak, et al [8] in the research to determine the effect of binder properties on the morphology of the powder bed. Binder solutions (2%, 5%, 10% w/w) of hydroxypropyl-cellulose (HPC) were prepared by gently stirring HPC-SL (Nisso Soda Co. Ltd., Tokyo, Japan) into deionized water at a constant rate. The stirring occurred overnight to allow proper degassing and hydration of the solution. Higher concentration of HPC mixed in deionized water results in a higher viscosity of binder. Binder properties were extrapolated from data provided from the Nisso Soda Co. Ltd. Website and given in Table 1.

Table 1: Binder viscosity	at specifid	concentrations.
---------------------------	-------------	-----------------

Viscosity (mPa*s)	Concentration (%)
7.00	2.0
40.0	5.0
85.0	8.0
200.0	10.0

Dimensionless values of binder drops are useful for predicting the printability of a drop [9]. Supplemental data such as dynamic viscosity μ and surface tension γ were found through data provided by the Nisso Soda Co. Ltd. website as well as the previous study performed by Rajniak [8]. The Reynolds number is defined in Equation 1:

$$Re = \frac{\rho dV}{\mu} \tag{1}$$

where ρ is the density of the binder fluid, d is the binder drop diameter, and V is the drop impact velocity. The Weber number is defined in Equation 2:

$$We = \frac{\rho dV^2}{\gamma} \tag{2}$$

The relationship between the Reynolds and Weber number are particularly valuable for determining drop printability. Through a reciprocation of the Ohnesorge number formula as given in Equation 3:

$$\frac{1}{Oh} = \frac{Re}{\sqrt{We}} \tag{3}$$

When the reciprocal of the Ohnesorge number is between 1 and 14, binder drops are observed to experience good jettability [10]. Table 2 documents these values for each of the tested binder drops, listed by viscosities of HPC.

Table 2: Binder viscosity with respective printability

Viscosity (Pa·s)	1/Ohnesorge
0.0122	18.98
0.0195	11.08
0.165	1.20

Although each concentration experiences different velocities by case and thereby different Reynolds and Weber numbers by case, the relationship between them (i.e., the reciprocal of the Ohnesorge number) remains constant. The powder used to jet the binder drops onto was also chosen to be HPC and has a mean diameter of $90 \mu m$.

There are other dimensionless parameters that must be determined to quantitatively analyze the relationship between the ejected height and length of binder powder after impact. These include the dimensionless height, width, and time. Nondimensional time t^* can be derived from the formula presented in Equation 4:

$$t^* = \frac{t}{\sqrt{\frac{0.5\rho d^3}{\gamma}}} \tag{4}$$

This parameter relies on a discrete time value *t* that increases at a rate of 0.2ms given the sample frame rate of 5000fps. The parameter is also dependent on drop density and surface tension, so it will vary across the three drop viscosities.

Dimensionless height H^* and width W^* are found by simply dividing the given value by the ejected drop diameter, as presented in Equations 5 and 6.

$$H^* = \frac{h}{d} \tag{5}$$

$$W^* = \frac{w}{d} \tag{6}$$

An ideal printing case will have minimized values of H^* and W^* as better printing occurs when the powder in which the drop is impinged does not spread far. This result solves the constraint of low resolution in binder jetting AM. The relationship of these two parameters across time t^* should result in a parabolic relationship for H^* and a linear relationship for W^* , given the tendencies of vertical and horizontal velocities for an object.

B. Experimental Setup and High-Speed Imaging System

A custom impingement rig was constructed for binder drop release under the testing conditions as shown in Fig. 2. The impingement rig is responsible for simulating the binder drop jetting process [11] using a needle clamp stand, a 22-gauge needle, and a syringe pump (New Age NE-300).

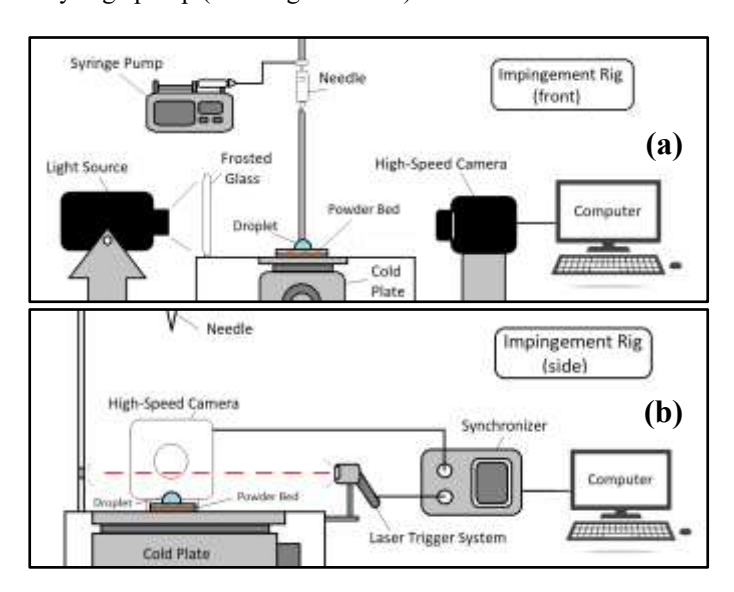


Figure 2: Experimental impingement rig as viewed from (a) the front and (b) the side.

The syringe pump is connected via tubing to a glass syringe filled with binder solution where it is consequently jetted onto the powder bed. This process is captured by a high-speed imaging system to investigate the interactions between the binder and powder upon impact. The height of the needle is adjusted to allow different impact velocities to be created. In the present study, three impact velocities are tested: 1.51m/s, 2.10m/s, and 2.59m/s.

A high-speed imaging system was implemented to capture the transient details of the complex binder-powder interactions. The high-speed imaging system consists of the high-speed camera (Photron FastCam WX-100), a laser trigger system (tachometer) to trigger the camera as the drop passes through, a synchronizer (BNC 575 Series) to connect the two devices, and a computer with the PFV4 software installed to record the images as the camera captured them.

An external light source is used to brightly illuminate the area of interest at the powder bed, while a sheet of frosted glass scatters the light to ensure an even spread of light in the captured images. All images were captured at 5000fps at a shutter rate of 1/10000s and resolution of 1280×512 pixels. The camera is set to center triggering mode

during recording to the PFV4 software. Additionally, all images were post-processed in the ImageJ software using contrast adjustment and a background removal algorithm.

III. Results and Discussion

A. High-speed Imaging of Binder Drop Impacting on a Powder Surface

Each of the three viscosities were tested at the three impact velocities to understand their relationship on the impingement of binder drops. These results are presented as image sequences sampled at 4ms intervals and grouped by impact velocity in Figs. 3-5.

Fig. 3 represents each of the viscosities at the lowest impact velocity of 1.51m/s. It is apparent that at the low velocity and low viscosity (0.0122 Pa·s) condition, the binder drop would not break upon impinging the powder surface. This case experiences a low rate of dry particle spread, i.e., ejected powder particles that did not absorb any binder. The low impact force of the impact also resulted in particle ejection trajectory that barely exceeded that of the drop size. Further, significant time elapses before the drop begins to eject powder.

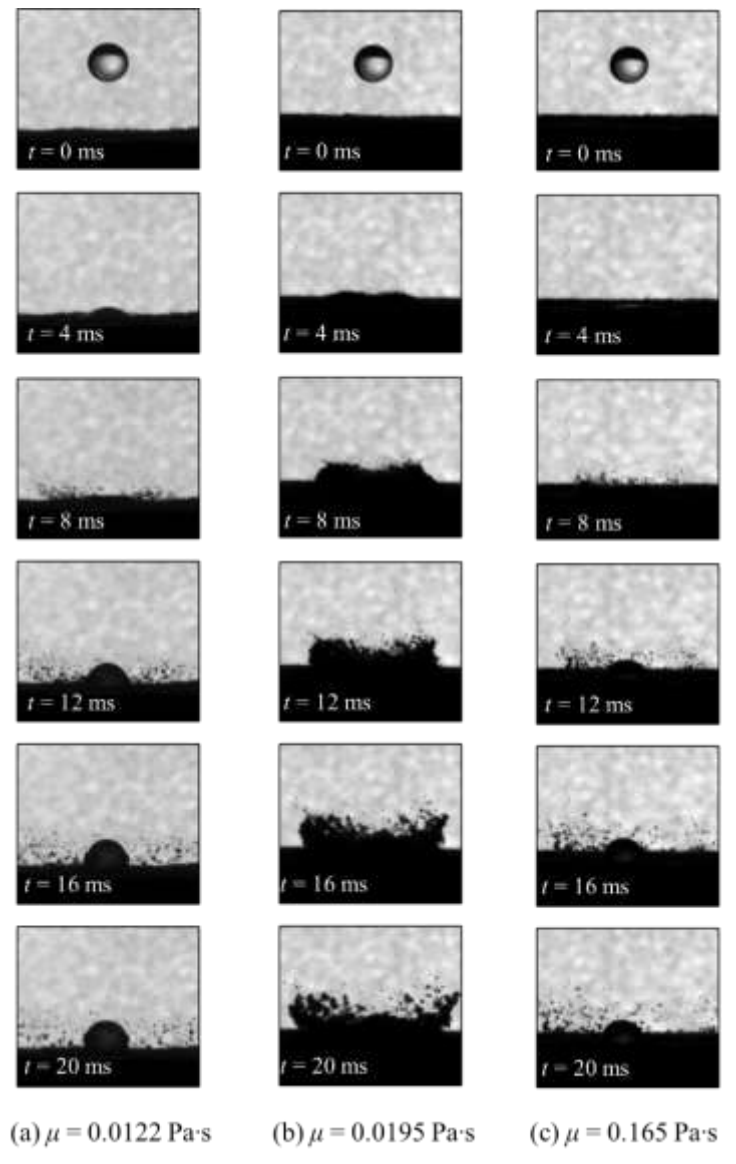


Figure 3: Snapshots of binder drop impacting on powder surface compared across the three viscosities at the impact velocity of 1.51m/s. Presented in columns from left to right, (a) 0.0122 Pa·s, (b) 0.0195 Pa·s, and (c) 0.165 Pa·s.

The binder drop with a higher viscosity (0.0195 Pa·s) experiences a significant increase in the number of binder-encapsulated particles compared to the low viscosity case. This leads to a noticeable absence of dry particles and a decreased ejection range after impact. Moreover, the combination of decreased particle ejection range and number of binder-encapsulated particles suggests that the given binder velocity and viscosity could be suitable for binder-jetting-based printing purposes. The relationship between the velocity and viscosity seem to dictate how efficiently a binder may perform upon impact.

As the binder drop viscosity increases to 0.165 Pa·s, the drop experiences a very low number of binder-encapsulated particles and low ejection spread. These results are consistent with the lowest viscosity than that of the intermediate viscosity. It is believed this phenomenon occurs because the lowest viscosity is unable to provide enough binder strength for significant granule growth (number of binder-encapsulated particles) and the highest viscosity is conversely too dense to spread over the particles. Conversely, the intermediate viscosity case (0.195 Pa·s) experiences the greatest number of binder-encapsulated particles after impact. The remaining viscosity cases experience a greater ejection range of both wet and dry particles instead.

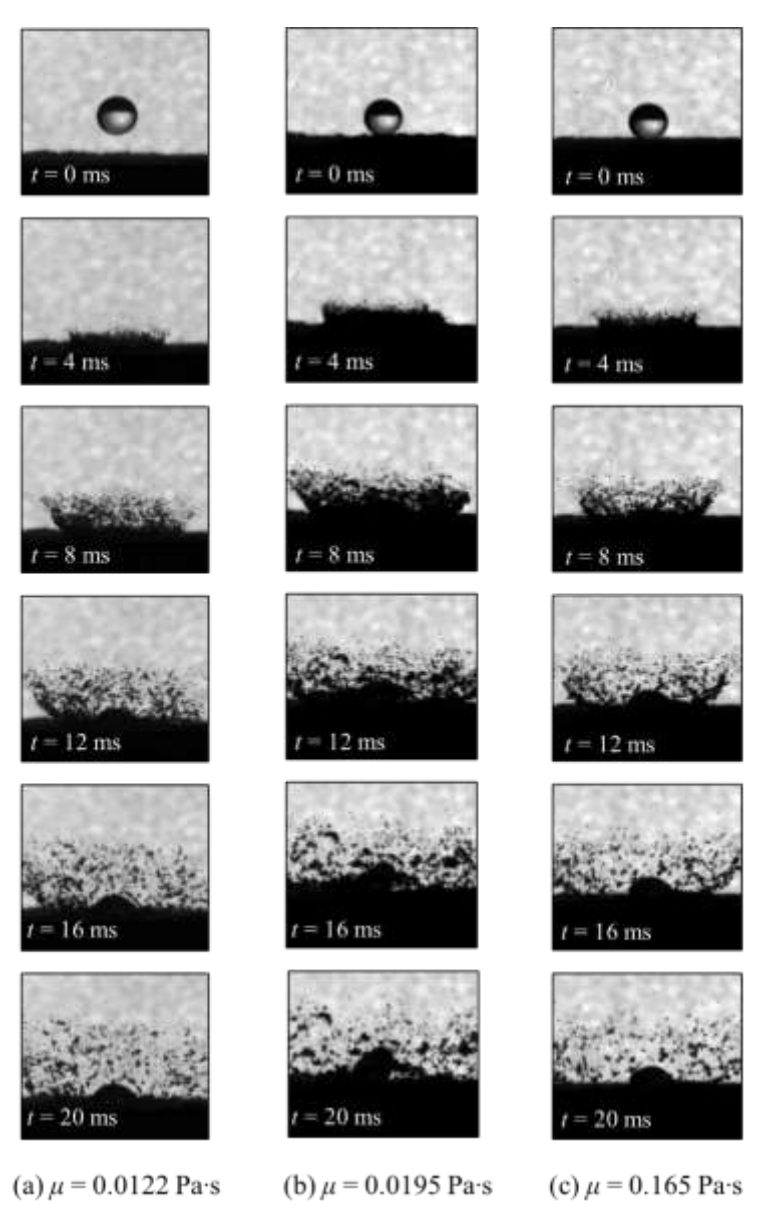


Figure 4: Snapshots of binder drop impacting on powder surface compared across the three viscosities at the impact velocity of 2.10 m/s. Presented in columns from left to right, (a) 0.0122 Pa·s, (b) 0.0195 Pa·s, and (c) 0.165 Pa·s.

Fig. 4 represents each of the viscosities at the intermediate velocity of 2.10m/s. Contrary to the lower velocity presented in Fig. 3, the effects of a higher impact velocity at the lowest viscosity result in interesting phenomena. The drop not only impinges and ejects powder at a quicker rate than the lower velocity, the ejected powder over doubles its previous launch height. The impact force from this increased velocity breaks the drop down further than the lower velocity case, as binder-encapsulated particles (i.e., ejected powder particles coagulated by binder) are more present after impact.

The case presented in Fig. 4b (intermediate viscosity) results in a much more disorderly impact than that of its low velocity case in Fig. 3. Unsurprisingly, the increase in impact velocity has greatly increased the ejection range of particles. The increase in velocity also seems to generate more dry particles at the expense of binder-encapsulated particles. Curiously, this effect resulted in the furthest spread of both wet and dry particles across all tested cases. It is also worth mentioning that instead of breaking or settling upon impact, this drop accumulated the powder of that around it. This is considered to be a tangible example of binder cratering, as demonstrated in Fig. 1(a).

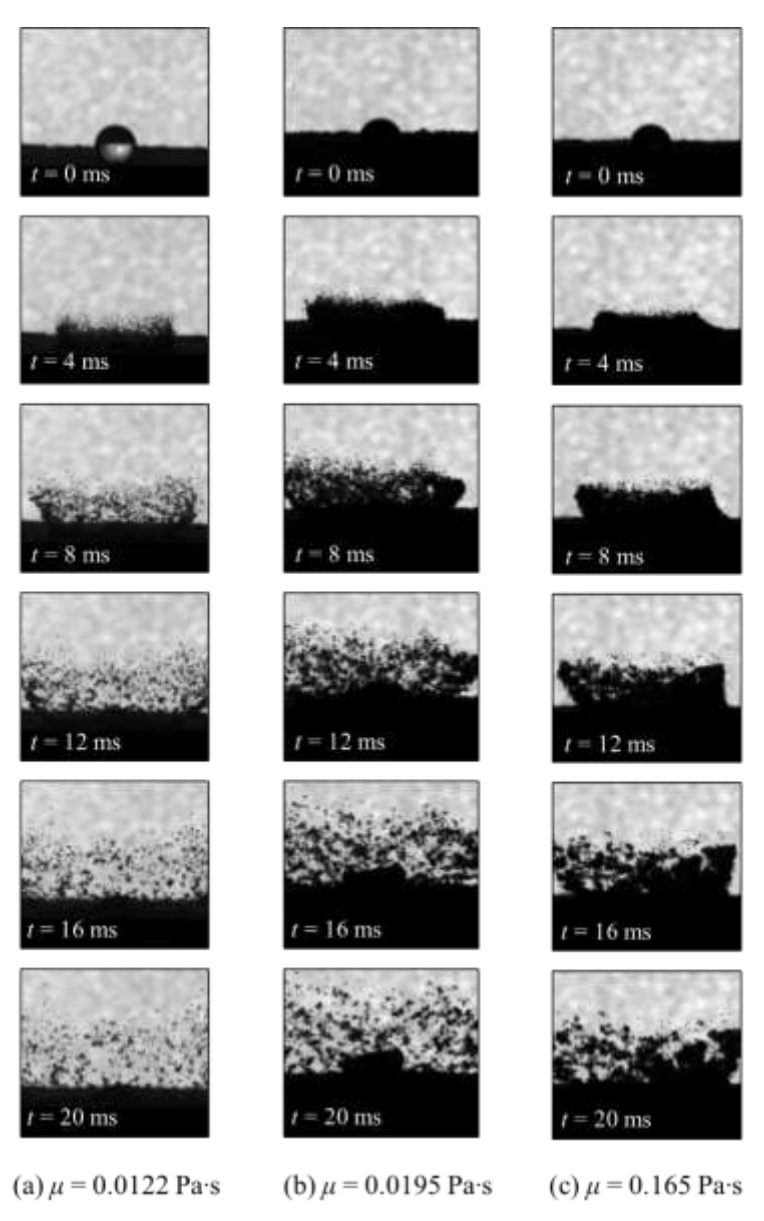


Figure 5: Snapshots of binder drop impacting on powder surface compared across the three viscosities at the impact velocity of 2.59 m/s. Presented in columns from left to right, (a) 0.0122 Pa·s, (b) 0.0195 Pa·s, and (c) 0.165 Pa·s.

At the low velocity and high viscosity case presented in Fig. 4c, the powder experiences a similar rate of ejection to that of the other viscosities at this velocity. There is a greater balance between wet and dry particles in this ejection. It is worth noting that the highest viscosity case did not experience the greatest printability of the three viscosities tested. Given that this viscosity case is at the lowest end of the printability spectrum, it can be concluded that certain parameters must continue to be adjusted to achieve more desirable results from this case.

Finally, the results from the highest viscosity case are presented in Fig. 5. As viscosities generally increase at higher velocities, there is more granule growth observed; it is therefore understood that there exists an ideal impact velocity for each viscosity of binder drop such that proper granule growth can occur. Further, increasing viscosity seems to correlate to a lessened spread of dry debris particles.

B. Extraction of Powder Ejection Parameters

All cases were captured at 5000fps in the high-speed imaging system to produce a series of frames for each of the cases. These frames were adjusted in ImageJ software to correct the images, largely concerning their brightness. These frames were then processed using a custom MATLAB code to determine the height and width of the ejected particle range at any given frame. An example case of this is provided in Fig. 6, where the 0.0195 Pa·s viscosity drop was impinged at 2.10m/s.

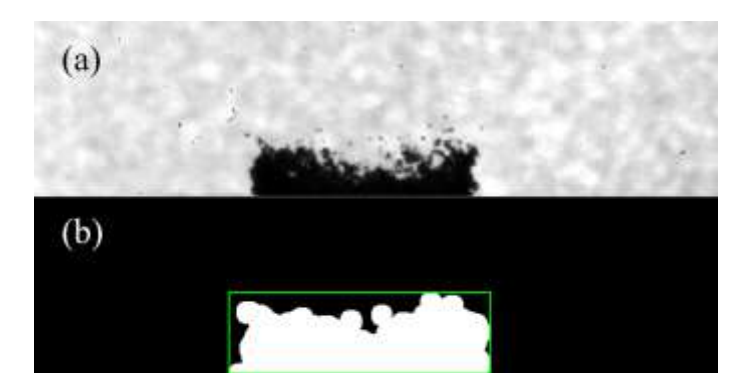


Figure 6: Image processing sample of the 0.0195 Pa·s binder drop at 2.10m/s. (a) The raw image of binder drop impacting the powder surface, and (b) The processed image.

The images undergo a binarization process where the largest "blob" of dark pixel values (i.e., the powder ejected, due to its contrast with the bright background) are identified and formed into larger disks as to maintain a continuous mass to assign a shape to. This mass is boxed in by the green bounding rectangle with a height and width equal to the height and width of the ejected powder measured in pixels. A calibrated image scale is used to correlate the pixels into tangible measurements such that the rectangle may provide real values of the ejection's height and width. This process is repeated for each frame of every case until there is a height and width for every instance of time.

Due to camera lens noise and inconsistencies in rising/falling patterns of the ejected particles, only small windows of time are graphically analyzed. Another issue in measurement occurs as ejected particle debris flies out of frame, so stagnant lines are created on the graph. Repeated experiments are advised to adjust camera settings as necessary so the full scope of ejection may be analyzed and processed to their complete potential.

C. Effects of Binder Viscosity on Ejection Dynamics

The nondimensionalized height and width for each velocity case are presented in Figs. 7-9 to better understand their relationship to viscosity over time. Ideal height and width behavior is to have minimized spread over the longest time so that inconsistencies are reduced in the printing process.

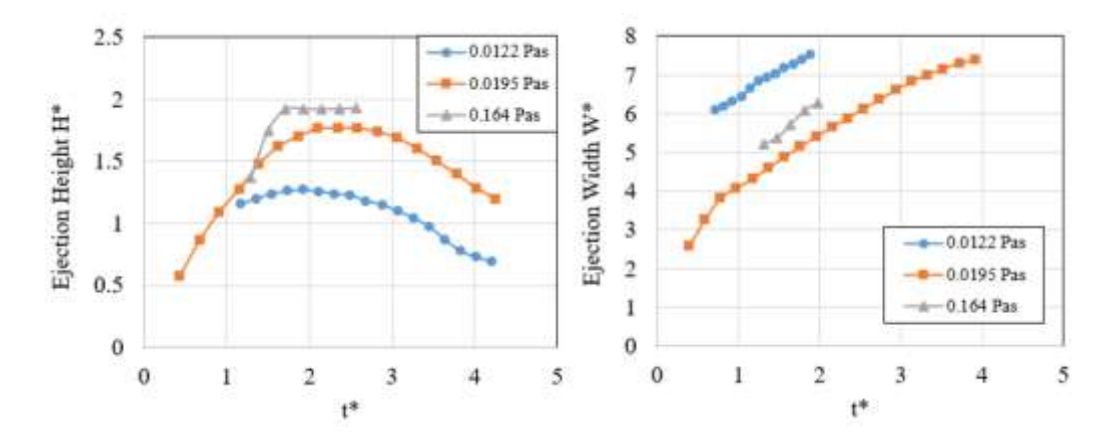


Figure 7: Nondimensionalized height (left) and width (right) for the impact velocity of 1.51m/s.

Fig. 7 denotes each of the viscosities plotted at the impact velocity 1.51 m/s. The intermediate viscosity case of 0.0195 Pa·s remains the most consistent data per its high amount of granule growth for easy tracking. For this reason does the case experience the slowest and smallest spread over time. These results align with what is expected of the trends due to the generally parabolic nature of the ejection height and the linear nature of the ejection width.

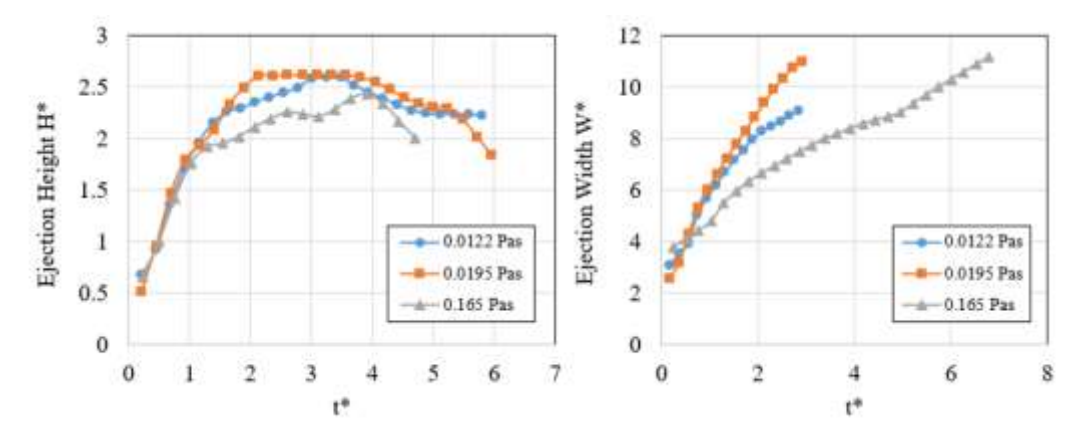


Figure 8: Nondimensionalized height (left) and width (right) for the impact velocity of 2.10m/s.

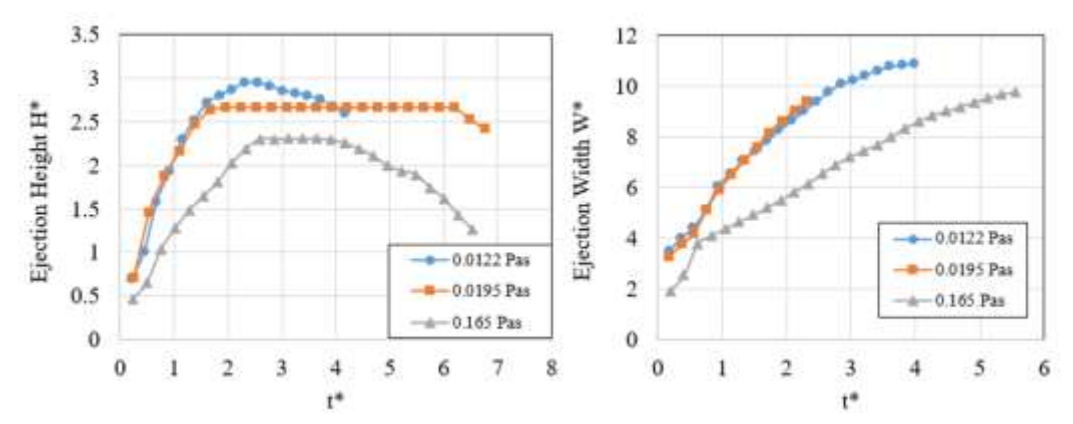


Figure 9: Nondimensionalized height (left) and width (right) for the impact velocity of 2.59m/s.

Fig. 8 analyzes the same viscosities but at the increased velocity of 2.10m/s. The increase in impact velocity has naturally led to an increase in the height and width and caused the trends to reach those values more quickly than that of the previous velocity. The key differences between Fig. 7 and Fig. 8 are that the two lowest viscosities now exhibit similar trends whereas the highest viscosity now experiences the lowest spread over time. This aligns with the theory

that there exists an ideal relationship between velocity and viscosity such that the ejected binder drop minimizes ejection spread while still binding the powder it impinges on.

The final velocity case analyzed in Fig. 9 contains an interesting trend where the increased velocity does not necessarily correlate to a further spread of powder. Much as the velocity increase in Fig. 8 improved the performance of the highest viscosity, this velocity increase continued to reduce height and width for the highest viscosity as well as executing it in a timelier fashion. The other two viscosities still align similarly. It is worth noting that no data is likely to exceed $H^* = 3$ or $W^* = 12$ due to the limitations of the camera framing.

D. 3.1 Effects of Impact Velocity on Ejection Dynamics

The relationship between velocity and the ejected powder are now to be compared in Figs. 10-12. These are graphed under the same parameters as Figs. 7-9 but plotted by velocities such that their results may be analyzed.

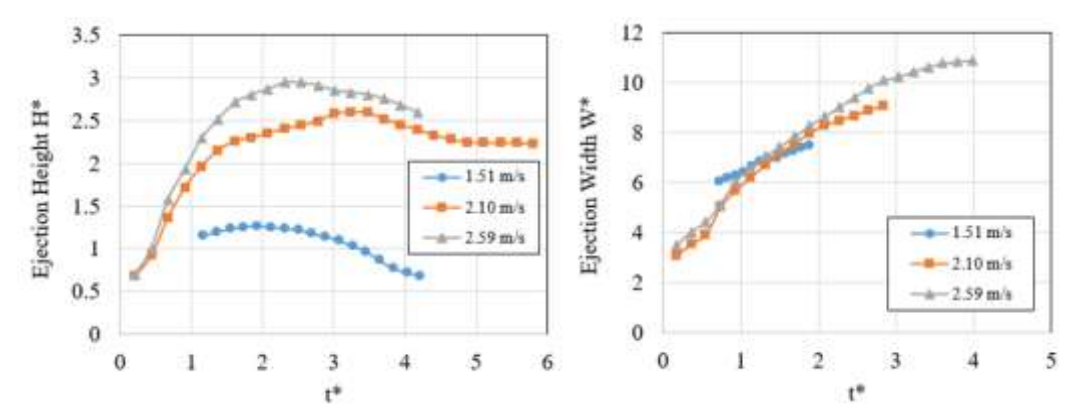


Figure 10: Nondimensionalized height (left) and width (right) for the binder viscosity of 0.0122 Pa s.

Fig. 10 presents the lowest viscosity case at all three tested impact velocities. The graphs comparing velocity are reasonable with what should be expected of an increase in impact speed: generally, an increase in impact velocity results in a higher and faster spread of powder after impact. This is especially evident in the ejection height results, where the increase nearly doubled from the impact velocity of 1.51 m/s to 2.10 m/s. The ejection width of the particles under this case are more similar than was expected from this experiment.

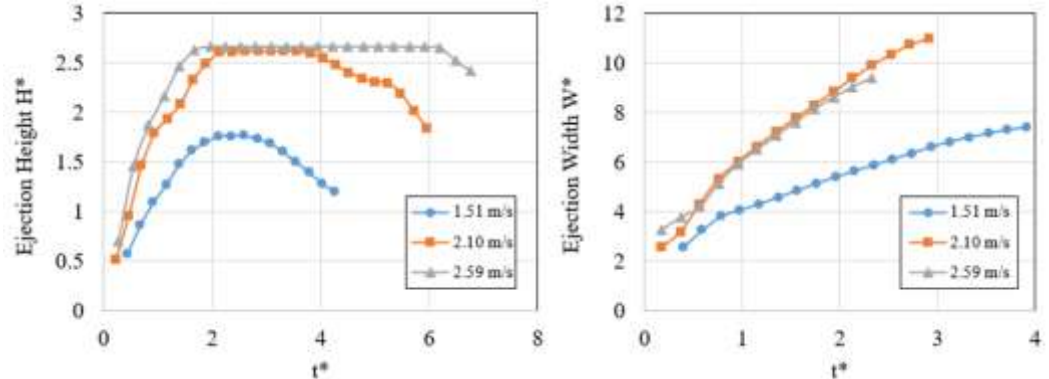


Figure 11: Nondimensionalized height (left) and width (right) for the binder viscosity of 0.0122 Pa s.

Fig. 11 presents the powder particle ejection dynamics for the intermediate viscosity case. The trends are largely similar between this data and Fig. 10. The relationship of height seems to exhibit a near identical behavior, especially considering the ideal patterns that the curves suggest the particles would follow. The two figures are even similar in how far and quickly the particles travel over time. The only significant difference is that the lowest impact velocity had a much smaller ejection width than the other cases with which it does not align.

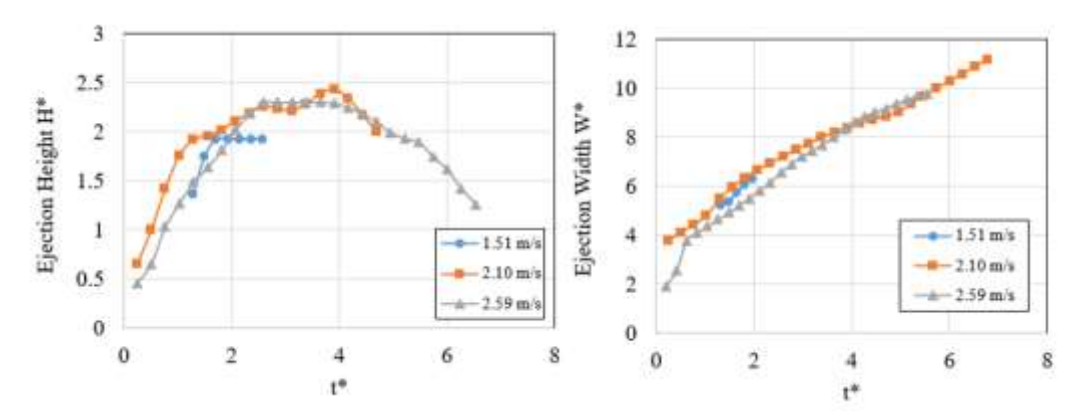


Figure 12: Nondimensionalized height (left) and width (right) for the binder viscosity of 0.165 Pa s.

Finally, the highest viscosity case is examined at all three velocities in Fig. 12. It is observed that the highest velocity case experiences the most ideal trends of smallest change over longest time, even though the data is largely consistent within itself. This final piece of evidence concludes that while impact velocity does play a key role in the interactions between binder and powder, it is not as strong an influence as binder viscosity.

Across all cases, it is generally observed that a greater impact velocity results in a greater amount of granule growth. This increase in impact velocity is also responsible for increasing the ejection range of binder-encapsulated debris particles while simultaneously decreasing the range of dry debris particles.

Therefore, it is concluded that the 5% concentration experiences the most efficient jettability as pertained to binder jetting AM. The 2% concentration case did not experience granule growth until the impact velocity increased, the effects of which negatively impacted the number of ejected particles after impact. This is a reasonable conclusion in agreement with the failed printability measurement in Table 2. Similarly, the 10% concentration was unable to bind the particles around impact until impact velocity increased to unsatisfactory amounts. This may also be attributed to its very low printability. The 5% concentration achieved a rather satisfactory amount of granule growth and minimal spread, especially apparent in the low impact velocity case. This is confirmed by the desirable printability number in Table 2 and is consistent with previous research, most notably that of Rajniak [1].

Further research is encouraged to study the interactions of binder and powder at other impact velocities and viscosities. It is also desired to quantify the flow dynamics of the binder during impact so that the jetting process may be better controlled.

IV.Conclusion

In the present study, the interactions between binder drop and powder bed were experimentally investigated as pertained to the viscosity and impact velocity of the drop. The experiments were conducted in a custom impingement rig under various test conditions (i.e., different impact velocities and binder viscosities). A high-speed imaging system was used to capture the transient details of the drop-powder interactions. It is found that an increase in drop impact velocity results in a greater range of particle ejection. A lower drop viscosity results in a higher dry spread of particles while a higher drop viscosity results in a greater number of binder-encapsulated particles. Across all cases, binder drops absorb particle granules at a rate inverse to their viscosity. It is also suggested that there is a direct relationship between the two parameters, range of ejected debris particles, and number of binder-encapsulated particles. The 5% concentration of binder experiences the most desirable jetting results.

Acknowledgments

The research work is partially supported by the City College of New York via faculty start-up funds. The support of National Science Foundation (NSF) under award number of CBET-2138214 is also gratefully acknowledged.

References

- [1] Shahrubudin, N., Lee, T. C., and Ramlan, R. "An Overview on 3D Printing Technology: Technological, Materials, and Applications." *Procedia Manufacturing*, Vol. 35, 2019, pp. 1286–1296. https://doi.org/10.1016/J.PROMFG.2019.06.089.
- [2] Lee, J. Y., An, J., and Chua, C. K. "Fundamentals and Applications of 3D Printing for Novel Materials." *Applied Materials Today*, Vol. 7, 2017, pp. 120–133. https://doi.org/10.1016/J.APMT.2017.02.004.
- [3] Oropallo, W., and Piegl, L. A. "Ten Challenges in 3D Printing." *Engineering with Computers*, Vol. 32, No. 1, 2016, pp. 135–148. https://doi.org/10.1007/S00366-015-0407-0/FIGURES/15.
- [4] Mostafaei, A., Elliott, A. M., Barnes, J. E., Li, F., Tan, W., Cramer, C. L., Nandwana, P., and Chmielus, M. "Binder Jet 3D Printing—Process Parameters, Materials, Properties, Modeling, and Challenges." *Progress in Materials Science*, Vol. 119, 2021, p. 100707. https://doi.org/10.1016/J.PMATSCI.2020.100707.
- [5] Gibson, I., Rosen, D., Stucker, B., and Khorasani, M. "Binder Jetting." *Additive Manufacturing Technologies*, 2021, pp. 237–252. https://doi.org/10.1007/978-3-030-56127-7_8.
- [6] Barui, S., Ding, H., Wang, Z., Zhao, H., Marathe, S., Mirihanage, W., Basu, B., and Derby, B. "Probing Ink-Powder Interactions during 3D Binder Jet Printing Using Time-Resolved X-Ray Imaging." *ACS Applied Materials and Interfaces*, Vol. 12, No. 30, 2020, pp. 34254–34264. https://doi.org/10.1021/ACSAMI.0C03572/ASSET/IMAGES/LARGE/AM0C03572 0007.JPEG.
- [7] Parab, N. D., Barnes, J. E., Zhao, C., Cunningham, R. W., Fezzaa, K., Rollett, A. D., and Sun, T. "Real Time Observation of Binder Jetting Printing Process Using High-Speed X-Ray Imaging." *Scientific Reports 2019 9:1*, Vol. 9, No. 1, 2019, pp. 1–10. https://doi.org/10.1038/s41598-019-38862-7.
- [8] Rajniak, P., Mancinelli, C., Chern, R. T., Stepanek, F., Farber, L., and Hill, B. T. "Experimental Study of Wet Granulation in Fluidized Bed: Impact of the Binder Properties on the Granule Morphology." *International journal of pharmaceutics*, Vol. 334, Nos. 1–2, 2007, pp. 92–102. https://doi.org/10.1016/J.IJPHARM.2006.10.040.
- [9] de Ruijter, M. J., de Coninck, J., and Oshanin, G. "Droplet Spreading: Partial Wetting Regime Revisited." Langmuir, Vol. 15, No. 6, 1999, pp. 2209–2216. https://doi.org/10.1021/LA971301Y/ASSET/IMAGES/LARGE/LA971301YF00005.JPEG.
- [10] Guo, Y., Patanwala, H. S., Bognet, B., and Ma, A. W. K. "Inkjet and Inkjet-Based 3D Printing: Connecting Fluid Properties and Printing Performance." *Rapid Prototyping Journal*, Vol. 23, No. 3, 2017, pp. 562–576. https://doi.org/10.1108/RPJ-05-2016-0076/FULL/PDF.
- [11] Bai, Y., Wall, C., Pham, H., Esker, A., and Williams, C. B. "Characterizing Binder-Powder Interaction in Binder Jetting Additive Manufacturing Via Sessile Drop Goniometry." *Journal of Manufacturing Science and Engineering, Transactions of the ASME*, Vol. 141, No. 1, 2019. https://doi.org/10.1115/1.4041624/367169.